A mucoadhesive-to-penetrating nanomotors-in-hydrogel system for urothelium-oriented intravesical drug delivery

Bin Zheng[1,2†], Haibao Zhang[3†], Jinxue Wang[4], Xiaowen Qin[1], Wentao Xu[5], Heng Wang[1], Zhenghong Liu[1], Yang Liu[1], Yixuan Mou[1], Wing-Fu Lai[6], Youqing Shen[7*], Dahong Zhang[1*] and Pu Zhang[1*]

Abstract

Intravesical therapy (IT) is widely used to tackle various urological diseases. However, its clinical efficacy is decreased by the impermeability of various barriers presented on the bladder luminal surface, including the urinary mucus layer and the densely packed tissue barrier. In this study, we report a mucoadhesive-to-penetrating nanomotors-in-hydrogel system for urothelium-oriented intravesical drug delivery. Upon intravesical instillation, its poloxamer 407 (PLX) hydrogel gelated and adhered to the urothelium to prolong its intravesical retention. The urea afterwards diffused into the hydrogel, thus generating a concentration gradient. Urease-powered membrane nanomotors (UMN) without asymmetric surface engineering could catalyze the urea and migrate down this concentration gradient to deeply and unidirectionally penetrate the urothelial barrier. Moreover, the intravesical hybrid system-delivered gemcitabine could effectively inhibit the bladder tumor growth without inducing any side effect. Therefore, our mucoadhesive-to-penetrating nanomotors-in-hydrogel system could serve as an alternative to IT to meet the clinical need for more efficacious therapeutics for urological diseases.

Keywords Mucoadhesive, Mucus-penetrating, Nanomotors, Intravesical therapy

Introduction

Intravesical therapy (IT) enables direct contact of a drug with a concentrated dose to the luminal surface of the bladder via a catheter and reduces the resulting systemic toxicity. It is commonly used as an adjuvant therapy after transurethral resection of bladder tumor, with its range of use having been expanded to tackle other urological diseases, including interstitial cystitis, overactive bladder, urinary incontinence, and chronic urinary tract infections [1]. However, the clinical efficacy of IT is limited, because the impermeable urothelial barriers, including the urinary mucus and the urothelium, hinder drug penetration. On the other hand, periodic voiding of urine facilitates the clear out of the drug during IT [2]. Therefore, a mucoadhesive-to-penetrating drug delivery system is imperative for IT to enhance drug retention and penetration in bladder tissues.

Generally speaking, such a dual-functional drug delivery system can be generated by encapsulating mucus-penetrating drugs into mucoadhesive formulations, which could be composed of nanofiber composites and pegylated nanoparticles, thiolated microspheres and

†Bin Zheng and Haibao Zhang contributed equally to this work.

*Correspondence:
Youqing Shen
shenyq@zju.edu.cn
Dahong Zhang
zppurology@163.com
Pu Zhang
zhangpuxjtuer@163.com
Full list of author information is available at the end of the article

Graphical Abstract
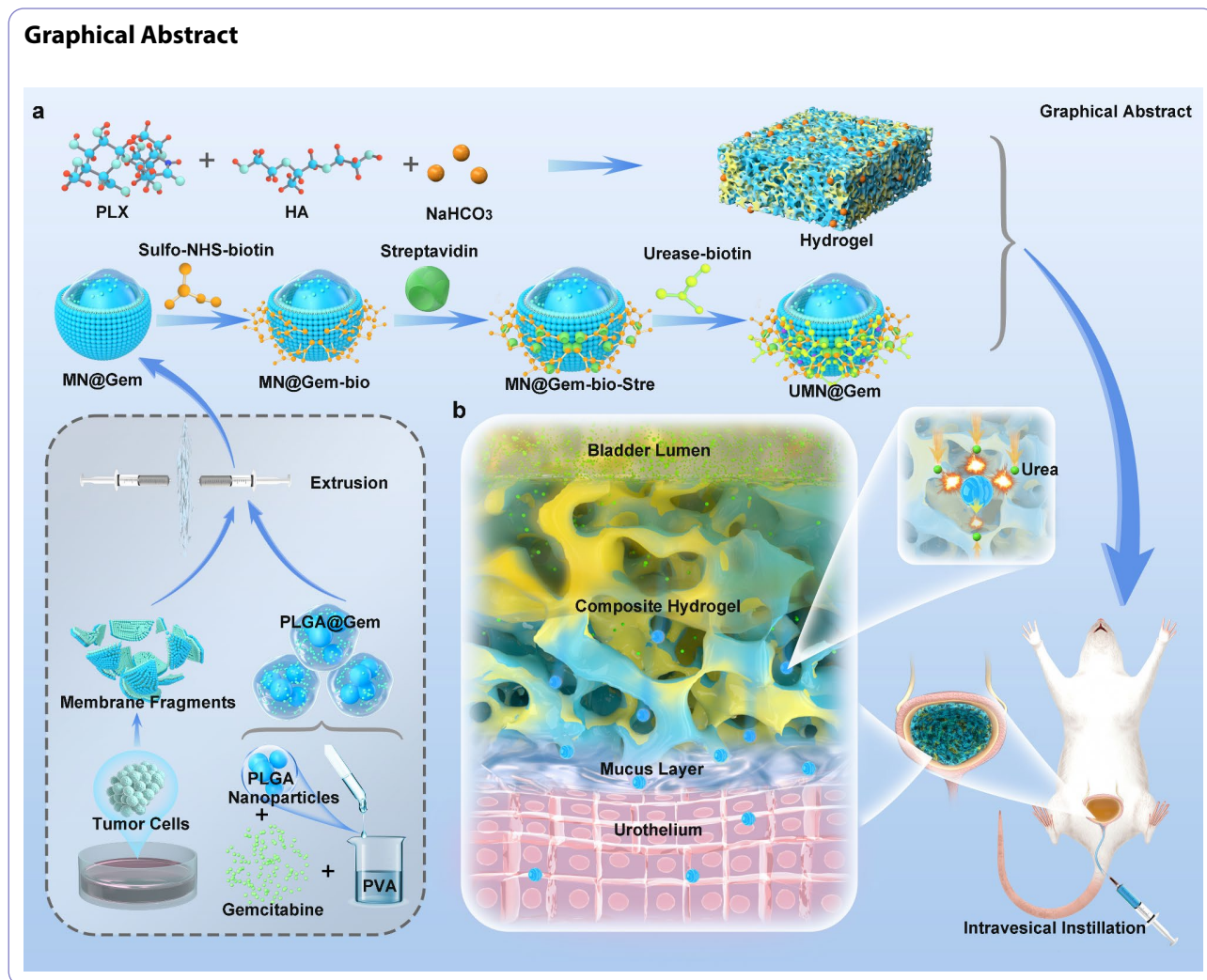
peptosomes, microgels and α-lac nanotubes, polymeric sponges and pegylated lipoplexes, or a post-expansile hydrogel foam and propylene glycol-embodying liposomes [3–7]. Upon intravesical instillation, mucoadhesive components bind to the urinary mucus to improve their intravesical retention, and afterwards the drugs transverse the mucus to penetrate into the urothelium. However, the non-fouling properties of mucus-penetrating components weakened their association with cells and hindered their further deep penetration into the urothelium [8]. In this study, we are the first group to report a mucoadhesive-to-penetrating system, composed of nanomotors and hydrogels, to achieve urothelium-oriented drug delivery. Upon intravesical instillation, PLX hydrogels (P) gelated and adhered to the urinary mucus [9] to prolong the intravesical retention, while concentrating the nanomotors onto the luminal surface. On the other hand, urease-powered nanomotors catalyze urea to enhance their mobility [10], with asymmetric surface engineering being a prerequisite to enhance their

directional mobility in general [11]. In this case, urea passively diffused into the P to generate a concentration gradient, down which urease-powered nanomotors without asymmetric surface engineering could migrate to effectively and unidirectionally penetrate the urinary barriers. Moreover, the intravesically instilled hybrid system-delivered gemcitabine displayed strong anti-cancer activity against orthotopic bladder tumors and well-tolerated biosafety (Scheme 1).

Results and discussion

The gelling properties of hydrogels composed of PLX, bicarbonate (BC), and hyaluronic acid (HA) are illustrated in Additional file 1: Fig. S1. At room temperature, P, P loaded with urease-powered membrane nanomotors (P@UMN), and P@UMN labelled with Coumarin-6 were in the sol state but underwent sol-gel transition upon exposure to 37 °C. The encapsulation of urease-powered membrane nanomotors (UMN) into the hydrogels did not affect the gelling properties. The disintegration of
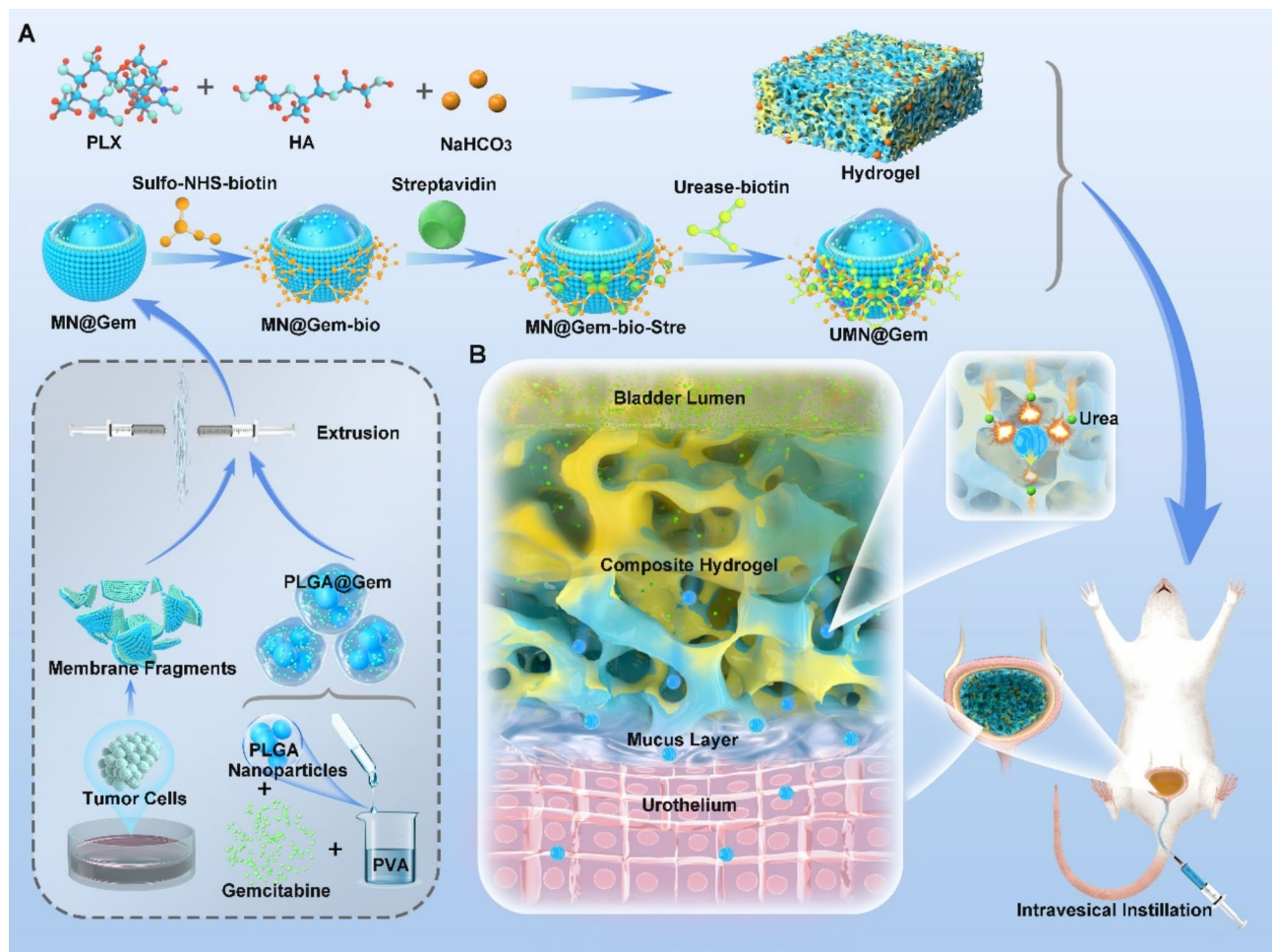
Scheme 1 A mucoadhesive-to-penetrating nanomotors-in-hydrogel system for urothelium-oriented intravesical drug delivery. **A** Gemcitabine-loaded PLGA nanoparticles and cell membrane fragments were co-extruded through liposome-extruder to form membrane-coated nanoparticles (MN), which were further surface engineered with urease via biotin-streptavidin-biotin linking. Urease-modified MN (UMN) was encapsulated into the hydrogel, composed of PLX, HA and sodium bicarbonate, to form a composite system. **B** The hybrid drug delivery system was introduced intravesically via a catheter. Upon intravesical instillation, its PLX hydrogel gelated and adhered to the urothelium to prolong its intravesical retention. Afterwards, UMN without asymmetric surface engineering could unidirectionally migrated from bladder lumen to urothelium, along down the urea concentration gradient within the hydrogel. As a result, it could deliver drugs deeply into targeted tissues

hydrogels is a prerequisite for their use in IT, because urinary tract obstruction induced by hydrogels may result in renal dysfunction [12]. To achieve this, in this study sodium bicarbonate was distributed throughout the gel, generating microbubbles to destroy the hydrogel integrity. The composite hydrogel disintegrated over time and completely dissolved in artificial urine (pH 6.5) after 4 h at 37 °C (Fig. 1A). Scanning electron microscopy (SEM) analysis indicated that the composite hydrogel presented a multi-porous structure with its pore size being approximately 5 μm, much larger than the diameter of UMN (Fig. 1B). Therefore, the diffusion of UMN within the composite hydrogel was not limited by steric hindrance. As displayed in Fig. 1C, the UV-Vis spectrum of UMN was overlapped with those of membrane nanoparticles (MN) and urease, indicating the successful loading of

ureases onto the surface of MN. The immobilized ureases on the particle surface did not lose their bioactivity (Fig. 1D). DLS analysis indicated that the average particle sizes of MN (in PBS buffer), UMN (in PBS buffer), MN (in artificial urine), and UMN (in artificial urine) were 214.7±1.1 nm, 216.1±0.5 nm, 215.0±0.7 nm, and 217.3ea1.2 nm, respectively (Fig. 1E). The zeta potentials of MN and UMN were −17.6±0.11 mV and −20.0±0.9 mV, respectively (Fig. 1F). The complex urine environment, usually hypotonic and acidic, impedes the stability of nanoparticles [13], but the average size and the size distribution of UMN remained almost unchanged during seven days of incubation in PBS buffer (pH=7.4) and in artificial urine (Fig. 1G and H). The cumulative release rates of gemcitabine (Gem) from MN-coated polylacticcoglycollic acid (PLGA) nanoparticles,
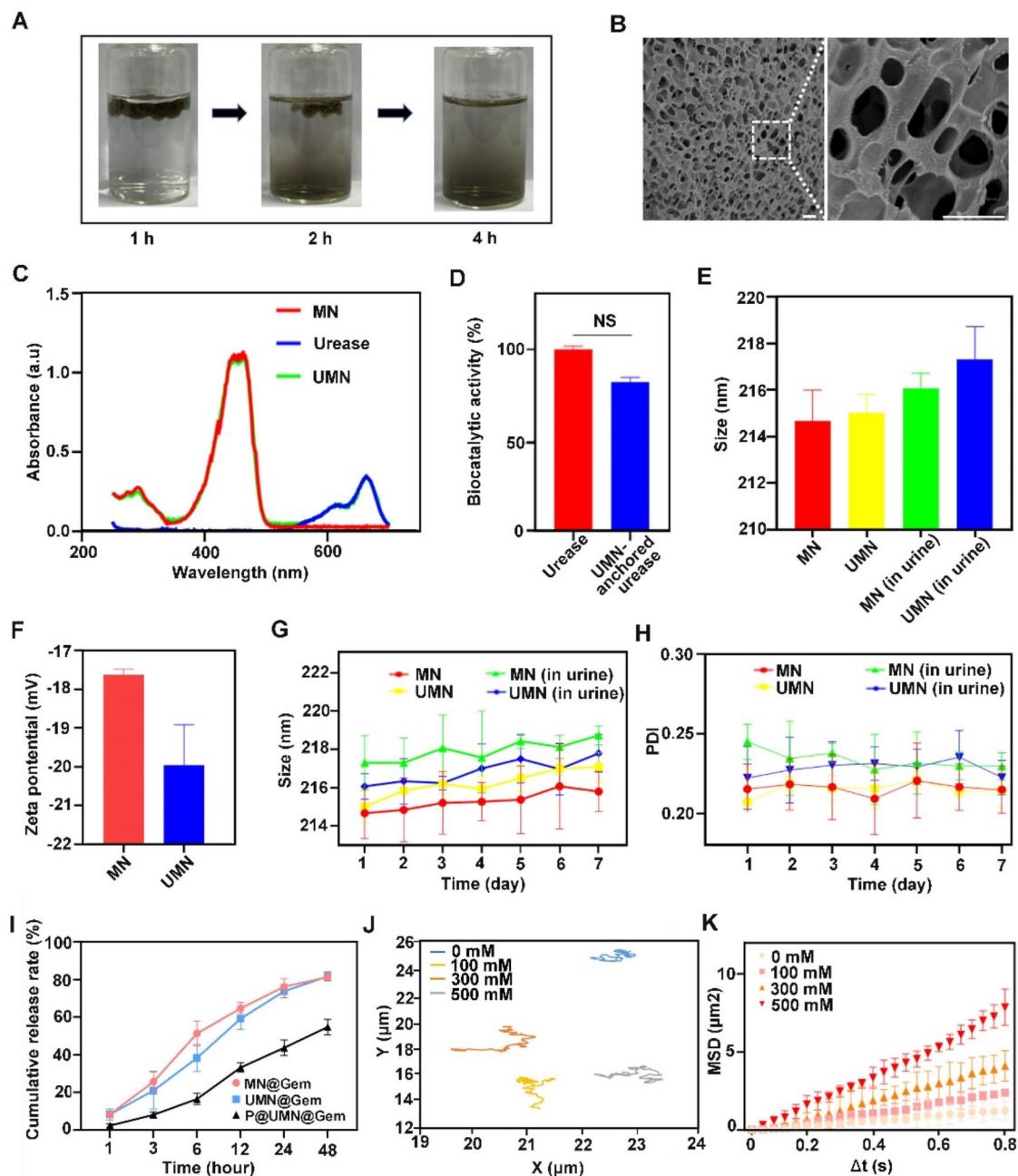
Fig. 1 Physicochemical properties of nanoparticles and hydrogels. **A** The self-disintegrating process of PLX hydrogel at 37 °C. **B** The morphology of PLX hydrogel observed by scanning electron microscope. The right inset was an enlarged part from the left inset. Scar bar: 1 μm. **C** The UV-vis spectrum of MN, urease and UMN. **D** Biocatalytic activity of urease and UMN-anchored urease (urease: 200U/mg). **E** The average particle size of MN, UMN, MN (in urine), UMN (in urine). **F** The average zeta potential of MN and UMN. **G** The change of the particle size of MN, UMN, MN (in urine), UMN (in urine) after timed incubation. **H** The change of the polydispersity index of MN, UMN, MN (in urine), UMN (in urine) after timed incubation. **I** Drug release profiles of Gem (Gem-eq dose: 20 μg/mL) from MN, UMN and P@UMN. **J** The trajectories of UMN (urease: 200U/ml) in simulated urine of different urea concentrations in 15s. **K** The mean-square displacement (MSD) analysis of UMN in simulated urine of different urea concentrations

UMN-coated PLGA nanoparticles and P@UMN-coated PLGA nanoparticles were 81.3±1.5%, 81.7±2.0% and 54.8±3.3%, respectively, after 48 h incubation in urine (Fig. 1I).

Recent studies have shown that the propulsion of synthetic motors can be triggered by biocatalytic conversion [14–16]. Urease-powered nanomotors convert urea into carbon dioxide and ammonia to lead to autonomous propulsion. For in vivo use, urine provides a sustainable source of urea (concentration up to 300 mM) [17] to power the motion of nanomotors. In simulated urine of low urea concentrations (0 mM, 100 mM, 300 mM), the trajectories of different nanomotors were tracked by using the optical tracking method. A linear increase of the mean-squared displacement (MSD) curve could be observed for UMN in 15 s (Fig. 1J) indicating that its diffusion fitted the typical pattern of Brownian motion. As the urea concentration increased to 500 mM, the motion of UMN showed directionality with a non-linear increase of the MSD curve (Fig. 1K), which was attributed to the self-propulsion effect. Although a molecular unbalanced distribution of ureases on the micro-/nanostructures is sufficient for the generation of net motion of particles, geometrically asymmetric micro-structures can undergo unidirectional motion more efficiently [18]. In this case, geometrical asymmetry was generated by unbalancing the distribution of urea on the particle surface, which was symmetrically functionalized with ureases.

Next, the unidirectional motility of nanomotors in different formulations across various urinary barriers was evaluated. The urinary mucus serves as the first impermeable barrier against intravesical drug penetration. The porcine bladder mucus was poured into the upper Transwell chamber to form an artificial mucus layer with the thickness of approximately 2 mm, and nanoparticles were loaded over the mucus layer followed by the loading of urea solution on the top. The transmucosal diffusion of nanoparticles was accelerated as the urea concentration increased, and nanoparticles in P@UMN went across the artificial mucus most rapidly under the urea concentration of 500 mM, with their transmucosal portion being 1.3–5.5 times higher than that of nanoparticles in other formulations (Fig. 2A-C). When urea was distributed evenly throughout the composite hydrogel in
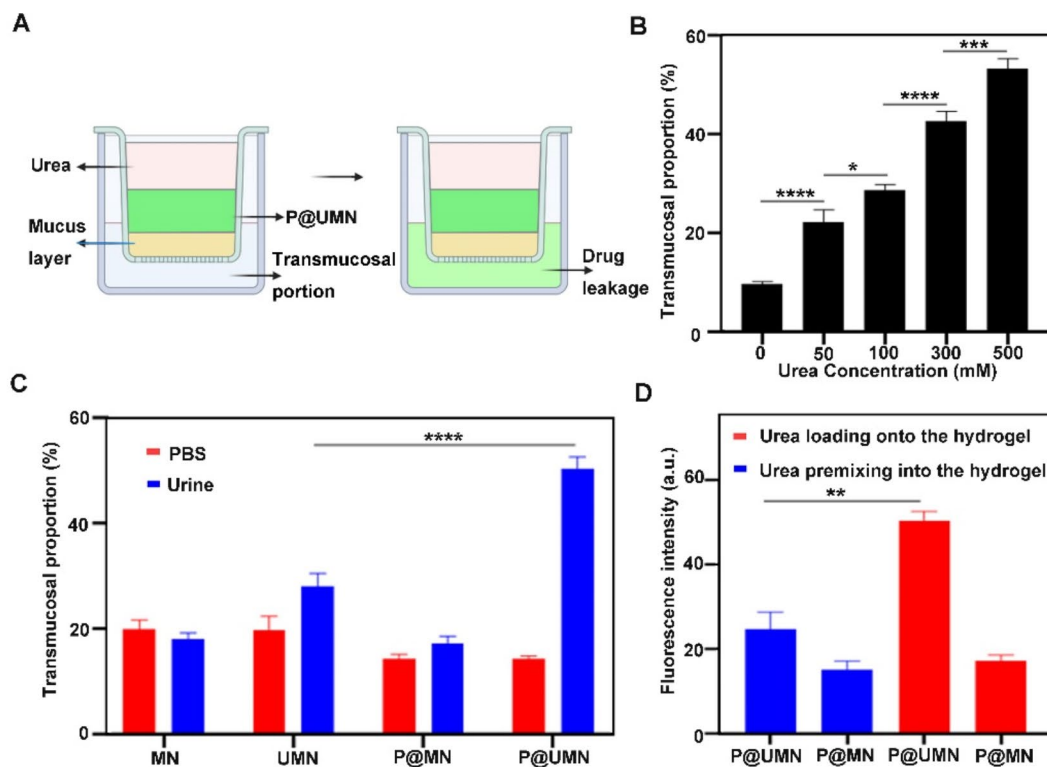
Fig. 2 The transmucosal transport of nanoparticles. **A** The Transwell assay was used to evaluate the mucus-penetrating efficiency of different nanoparticles encapsulated in the hydrogel. The nanoparticles distributed in the lower chamber represented the portion, which successfully transversed the mucus (mucus thickness: 2 mm. Coumarin-6-eq dose: 4 mg/ml, 2 h-coincubation). **B** The transmucosal transport of P@UMN (Coumarin-6-eq dose: 4 mg/ml) at different urea concentration, illustrated by the Transwell diffusion assay in (a). **C** The transmucosal transport of different nanoparticles (Coumarin-6-eq dose: 4 mg/ml) at urea concentration of 300 mM, illustrated by the Transwell diffusion assay in (a). **D** The transmucosal transport of P@UMN across the mucus under different conditions, illustrated by the Transwell diffusion assay in (a). * $p < 0.05$, ** $p < 0.01$, *** $p < 0.001$, **** $p < 0.0001$

the beginning of the Transwell diffusion assay, the diffusion of nanoparticles in P@UMN towards the lower Transwell chamber was significantly inhibited whereas that for nanoparticles in P@MN remained unchanged (Fig. 2D), demonstrating that the unidirectional nanoparticle motion was eliminated by urea redistribution, rather than the disruption of the structural integrity of the urea-incorporated composite hydrogel. The unidirectional motility of nanomotors in the composite hydrogel under no gravity was further investigated. The composite hydrogel was prepared as a cylinder with a pool in the middle to accommodate urea solutions (Fig. 3A). The concentration

of urea along the radius decreased from the inner part to the outer part after 1 h urea diffusion (Fig. 3B). After distributing nanoparticles evenly throughout the composite hydrogel, the urea concentration gradient triggered the redistribution of nanoparticles within the composite hydrogel (Fig. 3C). The UMN originally locating at the inner region could migrate to the outer region but MN could not. The redistributed portion of UMN in the outer region increased as the urea concentration in the central pool increased, reaching nearly 50% under the urea concentration of 300 mM (Fig. 3D, Additional file 1: Fig. S2). Therefore, the urea gradient formed in the composite
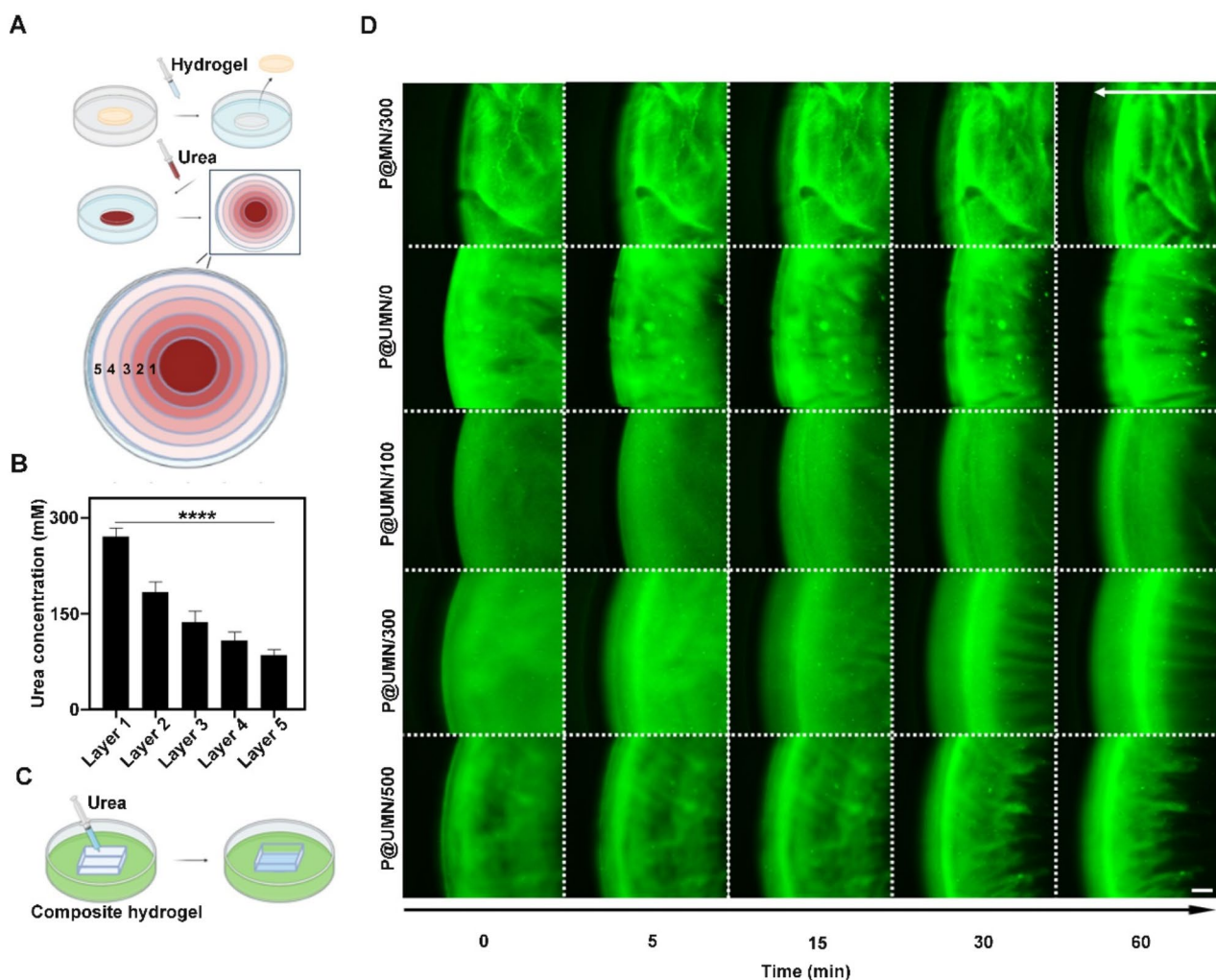
Fig. 3 The migration of nanoparticles down the urea concentration gradient. **A** The diffusion of urea in the composite hydrogel. The composite hydrogel with deactivated ureases was prepared as a cylinder with a pool in the middle to accommodate urea solutions (300 mM). **B** The concentration of urea distributed in different layers of the composite hydrogel from the inside out, illustrated by the urea diffusion assay in (a). **C** The redistribution of nanoparticles in the P@UMN or P@MN (Coumarin-6-eq dose: 2 mg/ml) under no gravity. The composite hydrogel with a concentration of 2 mg/ml coumarin-6 was prepared as a cylinder with a pool in the middle to accommodate urea solutions. **D** The redistribution of nanoparticles in the composite hydrogel at different time intervals, illustrated by the assay in (c). The white arrow showed the direction of nanoparticle migration. The number following the symbol '/' represented the urea concentration (mM) scale bar: 50 μm. **** $p < 0.0001$
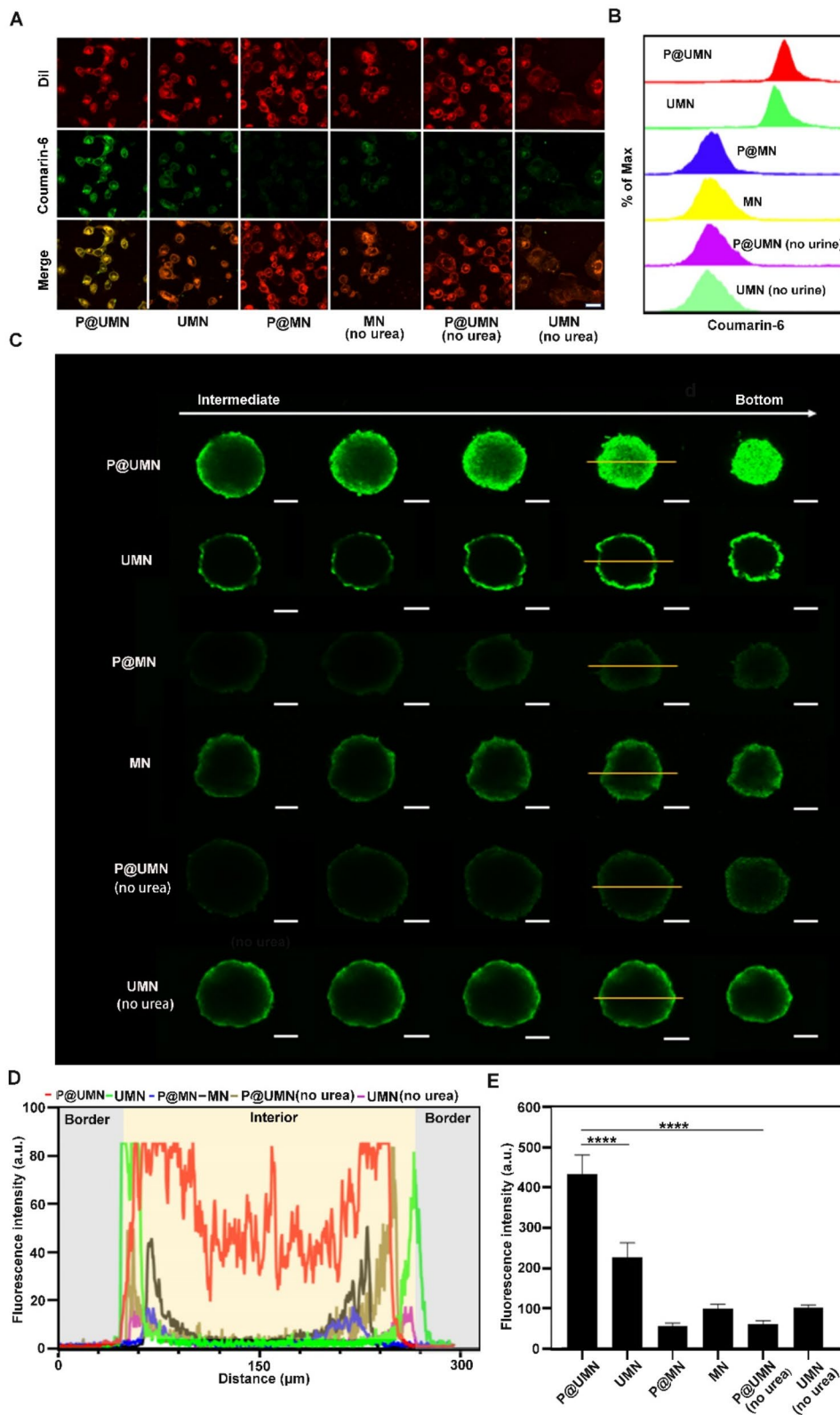
Fig. 4 (See legend on next page.)

Fig. 4 The transmembrane efficiency and urothelium-penetrating efficiency of nanoparticles. **A** CLSM analysis of the transmembrane efficiency of nanoparticles in T24 cells; scale bar: 25 μm (Coumarin-6-eq dose: 2 mg/ml, 2 h-coincubation). **B** Flow cytometry analysis of the transmembrane efficiency of nanoparticles in T24 cells (Coumarin-6-eq dose: 2 mg/ml, 2 h-coincubation). **C** The urothelium-penetrating efficiency of nanoparticles in SVHUC-1 multicellular spheroids. The Z-stack covered the course from the intermediate layer to the bottom layer at 100 μm intervals Scar bar, 100 μm. (Coumarin-6-eq dose: 2 mg/ml, 2 h-coincubation). **D** The distribution of different nanoparticles within T24 multicellular spheroids along the yellow line in (c), indicated by the Coumarin 6 fluorescence. **E**) Statistical analysis of the averaged Coumarin 6 fluorescence intensity in different T24 multicellular spheroids in (c). **** $p < 0.0001$

hydrogel is essential for the effective and unidirectional motion of urease-powered nanoparticles.

The urinary tissue is densely packed and stands as a solid barrier against the penetration of transmucosal drugs. The internalization of nanoparticles in T24 cells was analyzed by confocal laser scanning microscopy (CLSM) and flow cytometry. The transmembrane transport of Coumarin-6 via P@UMN or UMN under no urea stimulation was as slow as that via P@MN or MN, and could be facilitated by urea stimulation (Fig. 4A, Additional file 1: Fig. S3). Flow cytometry analysis confirmed that P@UMN under urea stimulation delivered Coumarin-6 into T24 cells most efficiently (Fig. 4B). In SVHUC-1 multicellular spheroids (MCSs), only P@UMN-delivered Coumarin-6 stimulated by urea penetrated into the inner region but Coumarin-6 in other formulations was limited to the superficial layer (Fig. 4C and D). As a result, the averaged Coumarin-6-fluorescence intensity of the MCSs in P@UMN group (treated with urea) was 1.9 times stronger than that in UMN group (treated with urea) and around 4.3–7.6 times stronger than those in other groups. The mucoadhesive-to-penetrating property of different drug delivery systems was further assessed in murine models which had received intravesical instillation for 2 h. P@UMN-delivered Coumarin-6 distributed throughout bladder tissues, including the outer serosa layer, but the infiltration of Coumarin-6 from other formulations was confined to the luminal surface of bladder tissues (Fig. 5A-E).

The anti-cancer effects of intravesical Gem in different formulations were evaluated both in vitro and in vivo. P (20 μg/ml), MN (0.4 mg/ml) and UMN (0.4 mg/ml) were non-toxic to T24 cells (Additional file 1: Fig. S4A-C). After encapsulating PLGA@Gem nanoparticles into UMN or P@UMN, P@UMN-delivered Gem displayed the strongest anti-cancer activity against T24 cells in a time-dependent and concentration-dependent manner, and its induced cytotoxicity was 2 times and 2.5 times stronger than that of P@MN-delivered Gem and free Gem at the Gem-equivalent dose of 20 μg/ml (Additional file 1: Fig. S5A and B), respectively. Murine orthotopic bladder cancer (BCa) models were intravesically treated with Gem in different formulations every 7 days for a total of five times. The bladder tumors shrunk when they first received the intravesical instillation of P@UMN delivered Gem, continued to be regressed after the following rounds of IT, and eventually got chemo-resected in four

of five cases, resulting in the tumor inhibition rate up to nearly 100%. Within the five-week follow-up, no tumor relapsed or progressed in those cases whose tumors were eradicated. However, free Gem barely impeded the tumor growth, and UMN-/MN-delivered Gem only inhibited the tumor growth at initial phase of IT with their therapeutic effect being obviously much weaker after the third IT (Fig. 6A and B). The body weight of mice in all groups increased at an initial period of IT but decreased in the PBS-treated group and the free Gem-treated group, with weight gain being observed in the other groups after the middle of IT (Fig. 6C). Histopathological analysis demonstrated that normal organs were not exposed to the toxicity of Gem in different formulations and orthotopic BCa was only eliminated by P@UMN-delivered Gem (Fig. 6D). Furthermore, there were no significant signs of liver dysfunction and renal dysfunction caused by IT in all groups (Fig. 6E). Taken together, P@UMN is an effective intravesical drug delivery system with well-tolerated biosafety.

Conclusion
In this study, we develop a mucoadhesive-to-penetrating nanomotors-in-hydrogel system for urothelium-oriented intravesical drug delivery. Upon intravesical instillation, the PLX hydrogel served as a mucoadhesive scaffold to concentrate UMN onto the luminal surface, and meanwhile the urea concentration gradient was formed within the hydrogel. UMN could catalyze urea to promote its mobility and unidirectionally migrated down the urea concentration gradient in the hydrogel to cross the urinary barriers, though not asymmetrically surface engineered with ureases. This hybrid system was capable of delivering intravesical drugs deeply into the urinary tissues and enhanced the anti-cancer activity of its loaded gemcitabine against bladder cancer.

Experimental section
Materials
PLX was provided by BASF Laboratories (Wyandotte, MI, USA). BC was supplied by Daejung Chemicals Co., Ltd. (Siheung City, Gyeonggido, Korea). HA (>1,000 kDa) was purchased from Thermo Fisher Scientific (Waltham, MA, USA). Urea colorimetric assay kits were bought from Elabscience Biotechnology Co., Ltd. Ethylacetate, PLGA, PVA and Urease were purchased from Macklin Biochemical Co., Ltd. (Shanghai, China). Gemcitabine
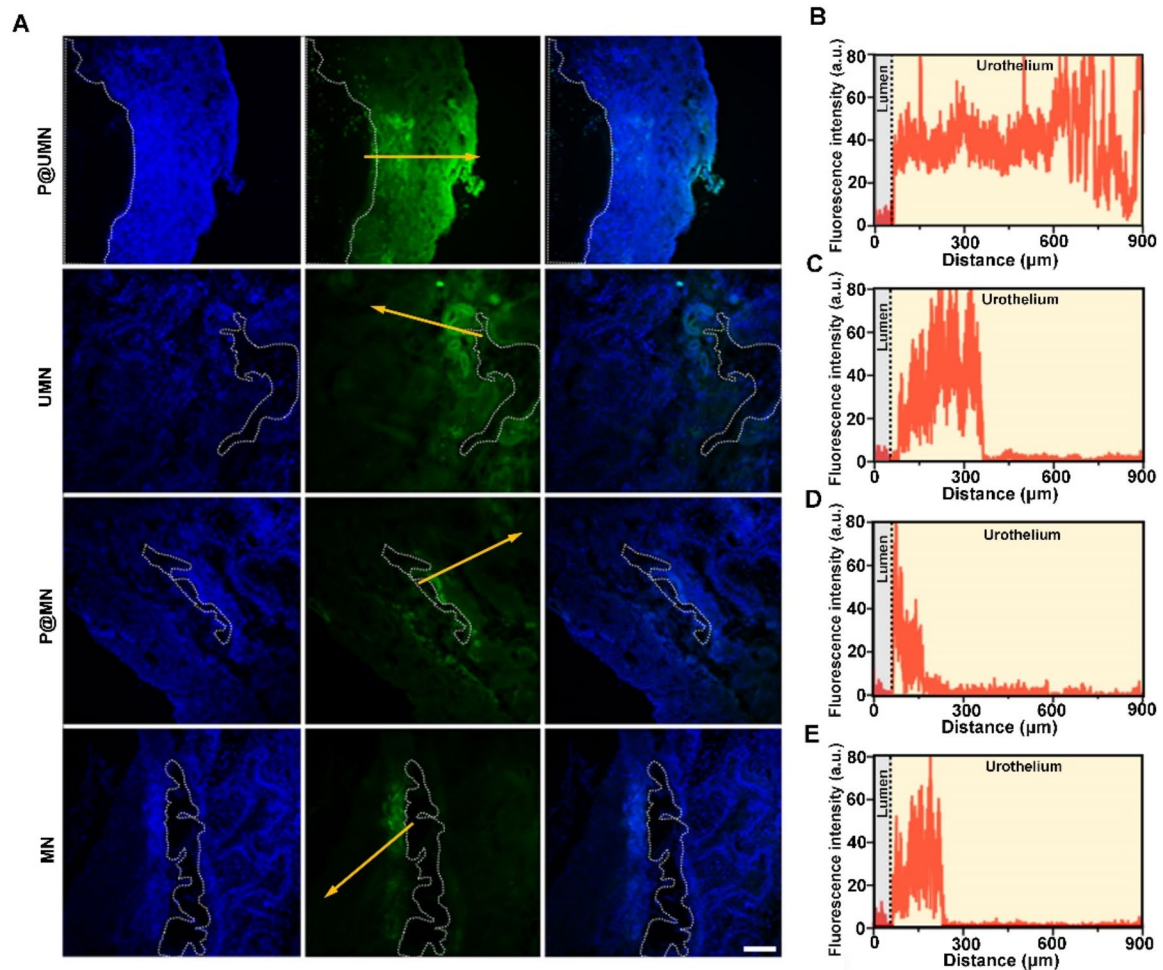
Fig. 5 The intravesical nanoparticle penetration in the urothelium. **A** The distribution of nanoparticles in the urothelium, as indicated by the Coumarin-6 fluorescence (green). The nucleus was stained with DAPI (blue). Scar bar, 100 μm. The areas surrounded by white dotted curve represented the bladder lumen (Coumarin-6-eq dose: 2 mg/ml, 2 h-coincubation). **B-E** The distribution of nanoparticles along the yellow axis in (a) from the bladder lumen to the urothelium

elaidate was purchased from MedChemExpress. Cell trackers such as Dil was purchased from Beyotime Institute of Biotechnology (Shanghai, China). Coumarin-6 was purchased from Sigma (Shanghai, China). Artificial urine were purchased from Solarbio Life Science Co., Ltd. (Beijing, China). DMEM (high glucose), penicillin–streptomycin, fetal bovine serum (FBS), and phosphate-buffered saline (PBS, pH 7.4) were obtained from Thermo Fisher Scientific (Waltham, MA, USA). Cell Counting Kit-8 (CCK-8) was purchased from Yeasen Biotech Co., Ltd. (Shanghai, China). Potassium fluorescein was purchased from LABLEAD. Inc. (Beijing, China) Isoflurane was purchased from RWD Life Science Co., Ltd. (Shenzhen, China).

Cell membrane fragments extraction
The T24 cells were washed twicewith PBS, scraped and resuspended in a hypotonic buffer to produce cell membrane fragments. The product was centrifuged at 700 ×g for 10 min at 4 °C and afterwards at 14,000 x g for 30 min at 4 °C to obtain the pure cell membrane fragments.

PLGA-Gem preparation
PLGA-Gem was prepared using the solvent evaporation method. PLGA (10 mg) and 1 gemcitabine elaidate (Gem, 1 mg) were dissolved in an organic solvent (ethyl acetate). The mixture was added dropwise into ultrapure water with vigorous stirring. Then, the mixture was added dropwise into a PVA solution followed by sonication. The
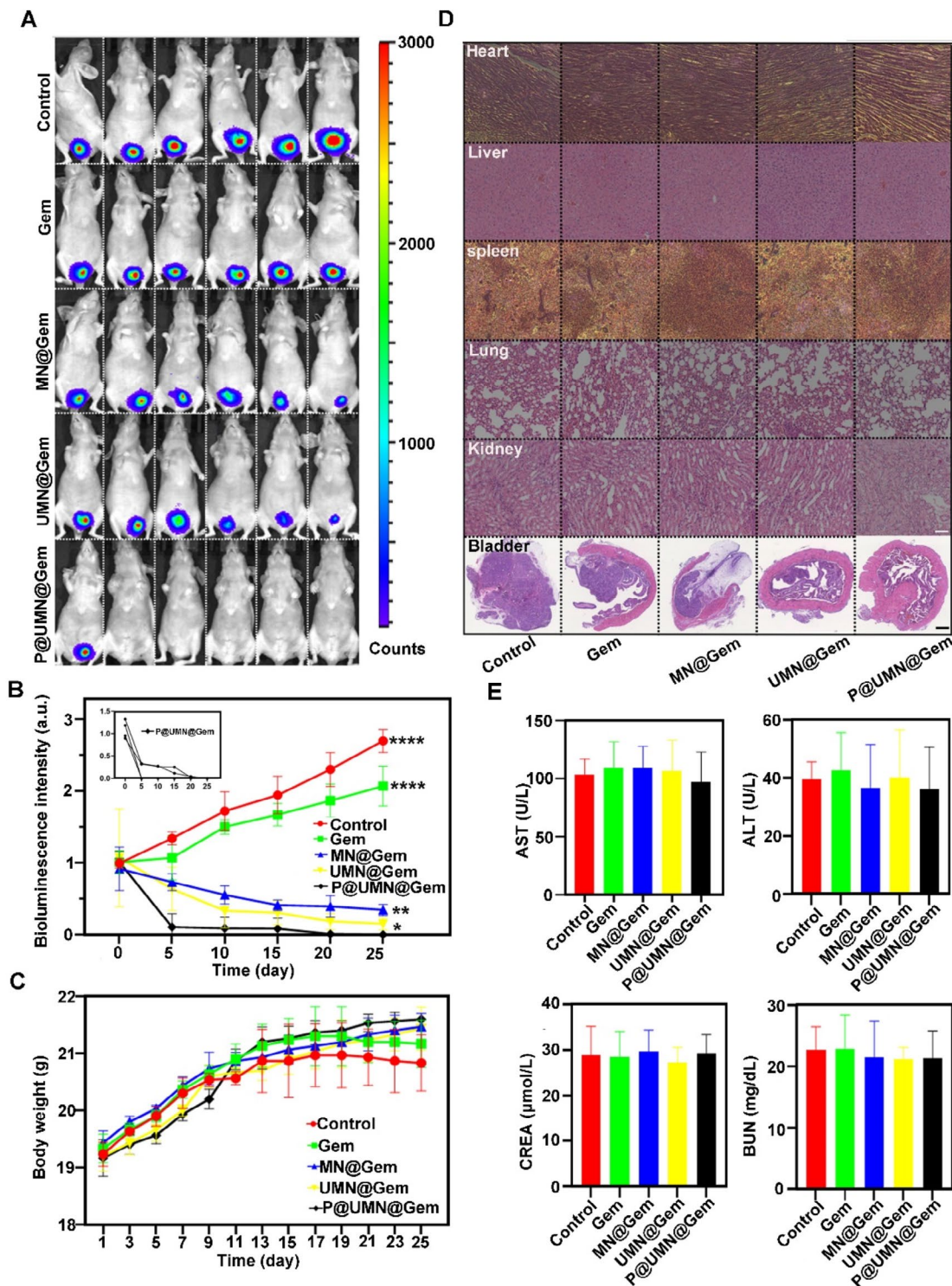
Fig. 6 Anti-tumor effect of nanoparticles in murine orthotopic BCa models. **A** In vivo bioluminescence analysis of anti-tumor activity of different formulations of Gem against orthotopic T24-Luci BCa (Gem-eq dose: 10 mg/kg, Intravesical instillation: 2 h). **B** The change of the averaged bioluminescence intensity of orthotopic BCa in different groups during intravesical therapy. The inset showed the individual change in bioluminescence intensity of orthotopic BCa in mice treated with P@UMN@Gem. **C** The change of the averaged body weight of murine in different groups during intravesical therapy. **D** Histopathological analysis of normal organs and bladder in different groups. Scar bar: 200 μm (normal organs), Scar bar: 1 mm (bladders). **E** Biochemistry analysis of blood extracted from different groups. $* p < 0.05$, $** p < 0.01$, $**** p < 0.0001$

volatile organic solvent was removed by evaporation. The drug loading content (DLC) and drug loading efficiency (DLE) of PLGA-Gem were calculated according to the following equations: DLC (%)=W(drug in PLGA-Gem)/ W(drug-loaded PLGA-Gem) × 100%; DLE (%)=W(drug in PLGA-Gem)/ W(total feeding drug) × 100%.

UMN@Gem preparation

PLGA-Gem (1 ml, 1 mg/ml) was mixed with the cell membrane fragments (0.3 mg) under vigorous stirring to envelope PLGA-Gem into the nanovesicles generated from the T24 cell membrane fragments. The mixture was transferred to a micro extruder (Avanti Polar Lipids) with polycarbonate film insertion (pore size: 400 nm). After repeated extrusion, the product was centrifuged at high speed and rinsed with sterilized ultra-pure water to obtain membrane coated PLGA-Gem nanoparticles (MN@Gem). Urease (1 mg /ml) dissolved in PBS (1x; pH 7.4, 200 µl) was incubated with Sulfo-NHS-biotin (200 µl; 16.6 µM) to generate biotinylated ureases (urease-biotin). Meanwhile, MN@Gem (200 µl, 1 mg/ml) was reacted with Sulfo-NHS-biotin (200 µl; 16.6 µM) to obtain biotinylated MN@Gem (MN@Gem-biotin). MN@Gem-biotin and urease-Biotin were purified 4 times with PBS through a 100 kda filter (Millipore) and centrifuged at 1500 RCF for 3 min. Streptavidin (20 µl; 166µM) was mixed with MN@Gem-biotin (20ul), and urease-biotin (20ul) was added after reaction for 1 h to obtain urease modified MN@Gem (UMN@Gem). High-speed centrifugation and three rounds of PBS washing are required to purify the UMN@Gem. The product was suspended in PBS and stored at 4 °C for use.

Preparation of self-disintegrating hydrogels

Self-disintegrating hydrogel was prepared by cold technique (PLX, HA-Schmolka, 1972). PLX was dissolved in distilled water (20%, w/v) at 4 °C under vigorous stirring. And then, BC was added into and reacted with the PLX solution under stirring at 4 °C overnight, followed by the addition of HA. The resulting PLX@BC@HA hydrogel (P) was stored at 4 °C for further use.

Preparation of hybrid drug delivery system

The UMN@Gem solution (1 ml) was centrifuged at high speed to obtain pure UMN@Gem, which were then dissolved into hydrogel P under viogorous stirring at 4 °C until the solution became transparent. The resulting product (P@UMN@Gem) was stored at 4 °C for future use.

Thermo-sensitivity analysis of hybrid drug delivery system

The gelling temperature of P and P@UMN@Gem were measured via the tube inverting test. In brief, the sample from each group (2 ml) was loaded into vials. These vials were put into water bath to increase the temperature from 25 °C to 37 °C. After that, the flowability of each sample was monitored by inverting the tubes.

Physicochemical characterization of hydrogels and UMN

P@UMN was dissolved into artificial urine (PH 6.5) at 37 °C to observe its gelation. The morphology of hydrogel P was observed by scanning electron microscopy (SEM, (SEM, Quanta 250FEG, FEI Co., Japan). Ultraviolet-vis-NIR (UV-vis-NIR) spectrum of the nanoparticles was obtained by using an UV-VIS-NIR spectrophotometer (Thermo Fisher Evolution 220, US). The particle size and Zeta potential of UMN and MN were measured via dynamic light scattering (DLS) techniques (Litesizer™500, AntonPaar, Graz, Austria). and change in the nanoparticle size was monitored to evaluate their stability in urine and PBS buffer.

CCK-8 assay

T24 cells were seeded into 96-well plates (5000 cells per well) and incubated for 12 h. T24 cells were treated with P@UMN@Gem (0.5–20.0 µg/ml), P (2–20 µg/ml) or MN@Gem (10–400 µg /ml) for 24–48 h, respectively. The medium in each well was then replaced with 0.2 ml of fresh medium containing 10% CCK-8 solution followed by 2-h incubation. The absorbance at 450 nm of each well was measured with a microplate spectrophotometer. Each experiment was independently repeated three times.

Mucus-penetration assay

The mucus from porcine bladders (Approval No:20221109172027655721) was collected and loaded onto the polyester membrane filter of a Transwell chamber (pore size: 0.4 µm) to generate an artificial mucus layer with the thickness of approximately 20 µm. Coumarin-6 was encapsulated into MN, UMN, P@MN and P@UMN for the convenience of observation. MN (100 µl), UMN (100 µl), P@MN (100 µl) or P@UMN (100 µl) was added to the upper chamber with the coumarin-6-equivalent dose being 4 mg/ ml, and then urea solution with different urea concentrations was gently onto the upper chamber. Meanwhile, the lower chamber was filled with 1 ml of PBS buffer. At different points in time, 100 µl of PBS buffer from the lower chamber was extracted for coumarin-6 fluorescence analysis. Fluorescence intensity was measured using a multi-mode microplate reader (Excitation/Emission: 464 nm/504 nm, Synergy Mx, Bio-Tek Instruments Inc., Winooski, US). The concentration of coumarin-6 was calculated according to a standard curve. Each experiment was independently repeated three times.

Urea diffusion assay and nanomotor migration assay

A baffle was placed in the center of the 6-well plate, and 3 ml of P@UMN solution (Urease inactivation) was poured into each well and gelated after heating up to 37 ℃. The baffle was gently removed to generate an empty chamber in the center of the well to accommodate urea solution with the urea concentration being 300 mM. After one-hour-incubation, different layers of the gelated P@UMN were harvested for the urea concentration analysis via a commercial kit. A baffle was placed in the center of the 24-well plate, and 1 ml of P@UMN and P@MN solution was poured into each well and gelated after heating up to 37 ℃. The baffle was gently removed to generate an empty chamber in the center of the well to accommodate urea solutions with different urea concentrations. In this case, coumarin-6 was encapsulated into all nanoparticles for the convenience of observation. The distribution of nanoparticles in the hydrogel was observed under an inverted microscope (TS 100, nikon Ti, Japan).

Endocytosis efficiency

T24 cells were seeded into a Petri dish (1×10^5 cells per dish) and were allowed to adhere for 12 h. And the cells were treated with P@UMN, UMN, P@MN, MN, P@UMN (no urea), UMN (no urea) for 4 h. The cells were labeled with Dil. The endocytosis of different nanoparticles were observed by a Confocal laser scanning microscopy (Leica TCS SP5 Confocal, Leica Inc., California, US), and ImageJ software was utilized for image analysis.

Tissue-penetrating efficiency in multicellular spheroid models

svhuc-1 cells were suspended in DMEM containing 0.12% w/v methylcellulose at a density of 1×10^6 cells per ml. Then, 25 µl of the cell suspension was dropped on the lid of a cell culture plate to form uniform droplets. PBS buffer (10 ml) was added to the plate to keep the droplets moist. After 72 h, dense spheroids were transferred to a low adhesion 96-well plate with one spheroid per well and incubated for an additional 72 h. The multicellular spheroid was treated with P@UMN, UMN, P@MN, MN, P@UMN (no urea), UMN (no urea). for 4 h, washed with PBS buffer three times and transferred for CLSM analysis. The Z-stack imaging was performed, covering the range from the intermediate layer of the spheroids to the bottom layer, with 100 µm intervals. Each experiment was independently repeated three times.

The distribution of different nanoparticle-delivered coumarin-6 in murine bladder after intravesical instillation

All animal procedures were approved by the Laboratory Animal Management Committee at Zhejiang Provincial People's Hospital (20230719143858450799).

All animal procedures were conducted in accordance with the guidelines of the Administration Committee of Experimental Animals in Zhejiang Province and the Ethics Committee of Zhejiang Provincial People's Hospital. Six- to eight-week-old nu/nu female mice were anesthetized by inhalation of 1% isoflurane in an oxygen gas mixture and kept on a heated platform during catheterization procedures. Lubricated angiocatheters were inserted into the urethra, and the bladder was flushed with 80 µl of sterile PBS. Coumarin-6 was encapsulated into MN, UMN, P@MN and P@UMN for the convenience of observation. Subsequently, 100 µl of P@UMN, UMN, P@MN, and MN (Coumarin-6- eq dose: 2 mg/ml) were intravesically instilled and preserved for 2 h, respectively. The bladder was washed twice with PBS. The mice were immediately sacrificed, and their bladders were harvested, frozen, and sectioned (20 µm thick) in a cryostat. The sections were examined using CLSM. ImageJ software was utilized for analysis.

Anti-cancer effect of different nanoparticle-delivered gem in murine orthotopic bca models after intravesical instillation

Six- to eight-week-old nu/nu female mice were anesthetized by inhalation of 1% isoflurane in an oxygen gas mixture and kept on a heated platform during catheterization procedures. Lubricated angiocatheters were inserted into the urethra. After full insertion, the bladder was flushed with 80 µl of sterile PBS. A 1-cm incision was made into the abdominopelvic cavity to expose the bladder. A single-cell suspension of 5×105 luciferase-transfected T24 cells in 50 µl of PBS was inoculated into the bladder wall. The needle passage was carefully controlled to penetrate through the inner layer of the bladder wall, allowing the cells to invade the bladder lumen. The incision was then closed layer by layer. Mice that developed hematuria one week after surgery were highly suspected of carrying BCa in situ. To compare the anti-cancer effects of different formulations of Gem, mice with orthotopic bladder cancer models were anesthetized with a mixture of 1% isoflurane and oxygen and kept on a heated platform. A lubricated vascular catheter was inserted completely into the urethra to empty the bladder. After two rounds of washing the bladders with PBS buffer (pH=7.4), Gem, MN, UMN, or P@UMN micelles with a Gem-equivalent dose of 10 mg/kg were intravesically instilled and preserved for 2 h. Throughout the procedure, the mice were kept under anesthesia, and the catheter was gently removed from the urethra. The mice were monitored daily for any signs of pain and distress. Intravesical instillation was performed every five days for a total of five times. The mice were weighed every 2 days. Mice were intraperitoneally injected with 100 mg/kg D-luciferin to monitor the in vivo bioluminescence of tumors using the

IVIS Spectrum system (IVIS Lumina XRMS Series III, PerkinElmer, PerkinElmer Inc., Waltham, US) every 5 days. Mice blood was obtained through the eye vein and subjected to blood biochemical analysis and blood panel testing. The mice were sacrificed one day after the final step of intravesical instillation, and the tissues (including bladder, heart, liver, spleen, lung, and kidney) were harvested for further histopathological examination by HE staining. The tissues were imaged using an inverted microscope (TS 100, Nikon Ti, Japan).

Statistical analyses

All experimental data were presented as mean±standard deviation (SD). Statistical analyses were performed using GraphPad Prism 9.0. The statistical significance was calculated using the Student's t-test. Statistical significance is indicated as $*P<0.05$, $**P<0.01$, $***P<0.001$, and $****P<0.0001$.

Supplementary Information

The online version contains supplementary material available at https://doi.org/10.1186/s12951-024-02816-7.

Supplementary Material 1

Data availability
No datasets were generated or analysed during the current study.

Declarations

Ethics approval and consent to participate
All animal procedures were approved by the Laboratory Animal Management Committee at Zhejiang Provincial People's Hospital (20230719143858450799). All animal procedures were conducted in accordance with the guidelines of the Administration Committee of Experimental Animals in Zhejiang Province and the Ethics Committee of Zhejiang Provincial People's Hospital.

Consent for publication
We give our consent for the manuscript to be published in Journal of Nanobiotechnology.

Competing interests
The authors declare no competing interests.

Author details
[1]Urology & Nephrology Center, Department of Urology, Zhejiang Provincial People's Hospital (Affiliated People's Hospital), Hangzhou Medical College, Hangzhou, Zhejiang, China
[2]Department of Urology, The First Affiliated Hospital of Jinan University, Guangzhou, Guangdong 510630, China
[3]Oncology Research Lab, Key Laboratory of Environment and Genes Related to Diseases, Ministry of Education, Xi'an Jiaotong University, Xi'an, People's Republic of China
[4]Center for Rehabilitation Medicine, Department of Neuroelectrophysiology, Zhejiang Provincial People's Hospital (Affiliated People's Hospital), Hangzhou Medical College, Hangzhou, Zhejiang, China
[5]Cancer Center, Department of Interventional Medicine, Zhejiang Provincial People's Hospital (Affiliated People's Hospital), Hangzhou Medical College, Hangzhou, Zhejiang, China
[6]School of Food Science and Nutrition, University of Leeds, Leeds LS2 9JT, UK
[7]Center for Bionanoengineering and Key Laboratory of Biomass Chemical Engineering of Ministry of Education, College of Chemical and Biological Engineering, Zhejiang University, Hangzhou, Zhejiang 310014, China

References
1. Palugan L, Cerea M, Cirilli M, Moutaharrik S, Maroni A, Zema L, et al. Intravesical drug delivery approaches for improved therapy of urinary bladder diseases. Int J Pharm X. 2021;3:100100–10.
2. Zhang P, Wu G, Zhang D, Lai WF. Mechanisms and strategies to enhance penetration during intravesical drug therapy for bladder cancer. J Control Release. 2023;354:69–79.
3. Krogstad EA, Ramanathan R, Nhan C, Kraft JC, Blakney AK, Cao S, et al. Nanoparticle-releasing nanofiber composites for enhanced in vivo vaginal retention. Biomaterials. 2017;144:1–16.
4. Zhao R, Du S, Liu Y, Lv C, Song Y, Chen X, et al. Mucoadhesive-to-penetrating controllable peptosomes-in-microspheres co-loaded with anti-mir-31 oligonucleotide and curcumin for targeted colorectal cancer therapy. Theranostics. 2020;10:3594–611.
5. Yuan Y, Liu Y, He Y, Zhang B, Zhao L, Tian S, et al. Intestinal-targeted nanotubes-in-microgels composite carriers for capsaicin delivery and their effect for alleviation of Salmonella induced enteritis. Biomaterials. 2022;287:121613–25.
6. Furst T, Dakwar GR, Zagato E, Lechanteur A, Remaut K, Evrard B, et al. Freeze-dried mucoadhesive polymeric system containing pegylated lipoplexes: towards a vaginal sustained released system for siRNA. J Control Release. 2016;236:68–78.
7. Li WZ, Zhao N, Zhou YQ, Yang LB, Xiao-Ning W, Bao-Hua H, et al. Post-expansile hydrogel foam aerosol of PG-liposomes: a novel delivery system for vaginal drug delivery applications. Eur J Pharm Sci. 2012;47:162–9.
8. Poinard B, Lam SAE, Neoh KG, Kah JCY. Mucopenetration and biocompatibility of polydopamine surfaces for delivery in an Ex vivo porcine bladder. J Control Release. 2019;200:161–73.
9. Baloglu E, Karavana SY, Senyigit ZA, Guneri T. Rheological and mechanical properties of poloxamer mixtures as a mucoadhesive gel base. Pharm Dev Technol. 2011;16:627–36.
10. Tang S, Zhang F, Gong H, Wei F, Zhuang J, Karshalev E, Esteban-Fernández de Ávila B, Huang C, Zhou Z, Li Z, Yin L, Dong H, Fang RH, Zhang X, Zhang L, Wang J. Enzyme-powered Janus platelet cell robots for active and targeted drug delivery. J Sci Robot. 2020;5:6137–47.
11. Ma X, Jannasch A, Albrecht UR, Hahn K, Miguel-López A, Schäffer E, et al. Enzyme-powered Hollow Mesoporous Janus Nanomotors. Nano Lett. 2015;15:7043–50.
12. Mou Y, Zhang P, Lai WF, Zhang D. Design and applications of liposome-in-gel as carriers for cancer therapy. Drug Delivery. 2022;29:3245–55.
13. Hamamoto S, Takemura T, Suzuki K, Nishimura T. Effects of pH on nano-bubblestability and transport in saturated porous media. J Contam Hydrol. 2018;208:61–7.
14. Jiang Z, Fu L, Wei C, Fu Q, Pan S. Antibacterial micro/nanomotors: advancing biofilm research to support medical applications. J Nanobiotechnol. 2023;21:388–403.

15. Lv Y, Pu R, Tao Y, Yang X, Mu H, Wang H, et al. Applications and future prospects of Micro/Nanorobots utilizing Diverse Biological Carriers. Micromachines. 2023;14:983–96.
16. Choi H, Cho SH, Hahn SK. Urease-powered polydopamine nanomotors for intravesical therapy of bladder diseases. ACS Nano. 2020;14:6683–92.
17. Liu L, Mo H, Wei S, Raftery D. Quantitative analysis of urea in human urine and serum by 1H nuclear magnetic resonance. Analyst. 2012;137:595–600.
18. Hortelão AC, Carrascosa R, Murillo-Cremaes N, Patiño T, Sánchez S. Targeting 3D bladder Cancer spheroids with urease-powered nanomotors. ACS Nano. 2019;13:429–85.

Publisher's note